# Interferometric Constraints on Spacelike Coherent Rotational Fluctuations

Jonathan W. Richardson,[1,2] Ohkyung Kwon,[3,4,*] H. Richard Gustafson,[5] Craig Hogan,[3,6] Brittany L. Kamai,[2,7,8] Lee P. McCuller,[9] Stephan S. Meyer,[3,10] Chris Stoughton,[6] Raymond E. Tomlin,[6] and Rainer Weiss[9,11]

[1]*Department of Physics, California Institute of Technology, Pasadena, California 91125, USA*
[2]*LIGO Laboratory, California Institute of Technology, Pasadena, California 91125, USA*
[3]*Department of Astronomy & Astrophysics and Kavli Institute for Cosmological Physics, University of Chicago, Chicago, Illinois 60637, USA*
[4]*College of Natural Sciences, Korea Advanced Institute of Science and Technology, Daejeon 34141, Republic of Korea*
[5]*Department of Physics, University of Michigan, Ann Arbor, Michigan 48109, USA*
[6]*Fermi National Accelerator Laboratory, Batavia, Illinois 60510, USA*
[7]*Department of Mechanical & Civil Engineering, California Institute of Technology, Pasadena, California 91125, USA*
[8]*Department of Astronomy & Astrophysics, University of California Santa Cruz, Santa Cruz, California 95064, USA*
[9]*LIGO Laboratory and Kavli Institute for Astrophysics & Space Research, Massachusetts Institute of Technology, Cambridge, Massachusetts 02139, USA*
[10]*Department of Physics, University of Chicago, Chicago, Illinois 60637, USA*
[11]*Department of Physics, Massachusetts Institute of Technology, Cambridge, Massachusetts 02139, USA*

(Received 15 December 2020; accepted 21 April 2021; published 14 June 2021)

Precision measurements are reported of the cross-spectrum of rotationally induced differential position displacements in a pair of colocated 39 m long, high-power Michelson interferometers. One arm of each interferometer is bent 90° near its midpoint to obtain sensitivity to rotations about an axis normal to the plane of the instrument. The instrument achieves quantum-limited sensing of spatially correlated signals in a broad frequency band extending beyond the 3.9-MHz inverse light travel time of the apparatus. For stationary signals with bandwidth $\Delta f > 10$ kHz, the sensitivity to rotation-induced strain $h$ of classical or exotic origin surpasses $\mathrm{CSD}_{\delta h} < t_P/2$, where $t_P = 5.39 \times 10^{-44}$ s is the Planck time. This measurement is used to constrain a semiclassical model of nonlocally coherent rotational degrees of freedom of spacetime, which have been conjectured to emerge in holographic quantum geometry but are not present in a classical metric.

DOI: 10.1103/PhysRevLett.126.241301

In this Letter, we report the results of an interferometric experiment designed to measure spatially coherent rotational fluctuations of a macroscopic system, on timescales faster than its light crossing time. The instrument, a reconfiguration of the Fermilab Holometer [1], consists of two colocated and coaligned $L = 38.9$ m long power-recycled Michelson interferometers, each operating at 1.3-kW power with a mean shot noise–limited sensitivity of $2.7 \times 10^{-18}$ m/$\sqrt{\mathrm{Hz}}$. The Holometer program is designed with two measurement configurations that collectively constrain a wide class of possible coherent spacelike fluctuations within a plane. For the first experiment [2–4], the light paths were entirely colinear and extended radially in orthogonal directions, as in gravitational wave detectors. In the present study, a new geometry is probed in which one arm of each interferometer is bent 90° near its midpoint to obtain an instrumental response to rotational modulations: rotations about an axis normal to the interferometer plane couple to the sensed degree of freedom, the differential arm length (DARM) $\delta l$, at high frequencies. Rotationally induced displacement would not have been detected in previous experiments.

The DARM signals of the two interferometers are sampled at 50 MHz. Each achieves shot noise-limited displacement sensitivity in a broad frequency band from 1.1 MHz to 20 MHz, extending beyond the 3.85-MHz inverse light travel time of the apparatus. The two DARM signals are cross correlated, averaging down below shot noise to a sensitivity of $6.1 \times 10^{-21}$ m/$\sqrt{\mathrm{Hz}}$ at 9.92 kHz resolution to stationary signals common to both interferometers. For each frequency bin, we average over $3.9 \times 10^{10}$ independent spectral measurements. In units of strain, $\delta h = \delta l/L$, our sensitivity to rotationally induced displacement noise surpasses a milestone $\mathrm{CSD}_{\delta h} < t_P/2$, where $t_P \equiv \sqrt{\hbar G/c^5} = 5.39 \times 10^{-44}$ s is the Planck time.

Our measurements are sensitive to a broad variety of coherent phenomena. In the context of a classical spacetime, they can constrain models of exotic new physical fields, including, for example, axionlike dark matter with a coherence scale comparable to or exceeding the apparatus size. Depending on the coupling mechanisms of the new fields, a cross-spectral signal can arise from a variety of correlated physical effects in the two interferometers [5]. Probing for possible phenomena beyond the framework of local field

 

theory, our measurements are used here to constrain a model of coherent, spacelike rotational fluctuations of spacetime, not described by local fluctuations of a classical metric, which can arise in a holographic quantum geometry [6,7].

It is not known how the spacetime locality built into classical relativity can be reconciled with quantum mechanics; the active gravity from the mass-energy of a nonlocal physical state leads to a breakdown of universal causal consistency [8]. Predictions for physical correlations at this intersection vary widely [9–17] and depend critically on the nature of macroscopic quantum coherence in geometrical states. For example, if classical spacetime emerges from thermodynamics of covariant causal structures [18,19], it is possible that all null surfaces, such as black hole horizons and light cones, represent nonlocally coherent quantum objects at all scales.

One estimate of spacetime fluctuations from holography [6,7,13,14], analogous to the standard quantum positional uncertainty $\langle \Delta x^2 \rangle > \hbar\tau/m$ of a mass $m$ over time $\tau$, is that a causal diamond surface of radius $R = c\tau$ fluctuates coherently with a variance $\langle (\delta R/R)^2 \rangle \sim t_P/\tau$, or a strain power spectral density of $t_P(\sim 10^{-44}\ \mathrm{Hz}^{-1})$ over a bandwidth $1/\tau$. This corresponds to the scale of coherent quadrupolar distortions a black hole horizon needs in order to radiate at the standard Hawking flux, one graviton of wavelength $c\tau$ per time $\tau$. This estimate is controversial because, due to the coherence on null structures, even Planck-scale uncertainties can create spacelike fluctuations of causal surfaces much larger than expected in standard local effective field theory and linearized gravity, by a factor $\sim\tau/t_P$.

In this Letter, we experimentally test one such model [7] in which correlated interferometer signal fluctuations arise from rotational uncertainties in the laboratory inertial frame as local spacetime is emergently defined from a quantum system without a background. The modeled instrument response to rotational uncertainty scales with a parameter normalizing the displacement spectral density, nominally $\eta \approx t_P$, connected to information limits on timelike world lines and their causal diamond boundaries. We constrain this parameter to $\eta < 0.25 t_P$ for models with one rotational axis; values much less than $t_P$ correspond to an information excess in violation of the holographic entropy bound. Our result still leaves untested general 3D models with two incompatible rotational observables, targeted by future experiments [20].

*Experimental design.*—The current bent-arm interferometers are a reconfiguration of the original instrument described in detail in Ref. [1]. The vacuum infrastructure, sensing and control system, and almost all optical components are carried over. We present an overview of the detector design with an emphasis on the changes made for rotational sensitivity.

The Holometer consists of two 38.9-m power-recycled Michelson interferometers, separated by 0.9 m beamsplitter to beamsplitter and coaligned. Figure 1 displays their layout. In each interferometer, continuous-wave $\lambda = 1064$ nm laser

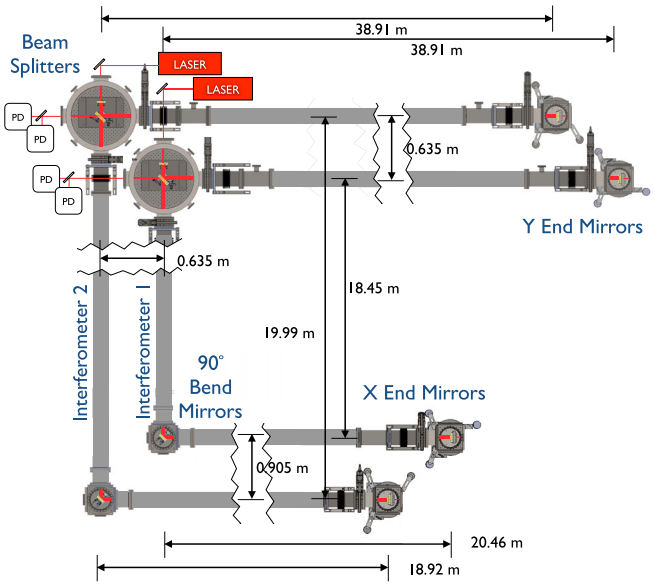


FIG. 1. Layout of the dual 40-m interferometer system. In this experiment, the X-arm of each interferometer is bent 90° near its midpoint. Dimensions are as marked, with the horizontal plane of interferometer 1 sitting 0.15 m higher than that of interferometer 2. The vacuum chambers are rendered with transparent tops; red lines indicate the positions of the laser beams, with heavier lines indicating the power-recycled cavity. Two radiofrequency photoreceivers sense the output intensity of each interferometer. A diagram of the post-detection signal flow is shown in Fig. 1 of Ref. [2].

light is injected to a beamsplitter and routed along two distinct optical paths to distant end mirrors, where it is retroreflected. The returning beams coherently interfere at the beamsplitter with an output intensity sinusoidally dependent on $\delta l$.

To produce a linear optical response to small DARM fluctuations, each interferometer is operated at an offset of approximately 1 nm from a dark fringe. A digital servo senses fluctuations in the power exiting the antisymmetric port and feeds back differential signals to piezoelectrically actuated end mirrors at frequencies up to 600 Hz [1]. It maintains 50 pm rms residual motion, as measured through the 16-kHz Nyquist frequency of the control system. The remaining power exiting the symmetric port is reflected back into the interferometer using a $T = 1000$ ppm transmission mirror. This mirror forms an overcoupled Fabry-Perot cavity with the interferometer whose 3.85 MHz free spectral range is determined by the average arm length. The input laser frequency is locked to the average arm length via the Pound-Drever-Hall technique [21], achieving a typical resonating power of 1.3 kW from 1.0 W of injected power. A separate radio frequency (rf) data acquisition system samples the interferometer output intensities at 50 MHz and computes their cross-spectral density in real time.

When the light propagates along entirely colinear paths extending radially, as in the original instrument, rotations

about an axis normal to the interferometer plane at the beamsplitter—the point of measurement—displace the end mirrors transversely to the optical axis, inducing no change in arm length. To obtain a first-order coupling of rotation to DARM, one arm of each interferometer is bent 90° near its midpoint, as illustrated in Fig. 1. In this configuration, such rotations displace both mirrors in each X-arm along its optical axis, resulting in a net arm length modulation at high frequencies. Although layouts more optimal for rotational sensitivity are possible, our design was chosen as a practical balance between infrastructure constraints, maximizing the reusability of the previous system, and the required integration time for a statistically conclusive model test. The reconfigured instrument also remains sensitive to purely translational, nonrotational displacements, but such sources were excluded to similar precision by the previous Holometer experiment [2,3] and their coupling strength here is smaller. Measured limits on the possible couplings of environmental rf noise are presented in the Supplemental Material [22]. Throughout, we quote our measurements in units of the effective linear arm length displacement, rather than in angular units, because the angular calibration is dependent on the model of rotationally induced displacement. For example, under the model tested here, the rotations are non–rigid body in nature [7]. The arm length displacement can also be readily converted to units of differential light phase via the multiplicative factor $4\pi/\lambda$.

Each 90° arm bend is implemented through the addition of a 2 inch diameter, 1/2 inch thick highly reflective mirror. The mirrors are fabricated from Corning 7980 0A low-inclusion fused silica substrates and polished to subnanometer flatness, with a 5 arc-minute wedge. They are coated for high $p$-polarization reflectivity at 45° incidence and have a measured transmission of $T < 10$ ppm. The interferometers do not have output mode cleaners, so a significant contrast defect reduces their sensitivity. To minimize the defect, the same coating is applied to both sides, mitigating distortions of the beam wavefront induced by mechanical stress in the coating. Each bend mirror is mounted in a Newport 8822-UHV two-axis picomotor mirror mount placed on a two-stage seismic isolation platform. The entire assembly is housed inside a 10-inch six-port vacuum cube. Similarly to the end mirror stations [1], high-frequency vibration reduction is achieved with a passive system of masses mounted on three 19 mm diameter Viton balls, here with two stacked stages using 10.5-kg steel masses. Each vacuum cube is mounted on a steel slab set on concrete footings originally used by the vacuum tubes of the straight-arm configuration. Along the new section of arm, the vacuum tubes are supported by new 0.3 m diameter concrete pillars set 1.9 m deep. The arm tubes are mechanically decoupled from the corner mirror stations using hydroformed stainless steel bellows. The two relocated end stations are mounted on separate steel plates, each weighing 2300 kg and resting on three 0.3 m diameter concrete pillars set 1.9 m deep.

*Measurement.*—The differential arm length signals of the two interferometers are sensed by photoreceivers at each antisymmetric port and synchronously digitized at 50 MHz. As in previous studies [2–4], the time series are characterized by their cross-spectral density (CSD), a measure of the correlated interferometer noise power,

$$\mathrm{CSD}[\delta l_1, \delta l_2](f) \equiv \int_{-\infty}^{\infty} \langle \delta l_1(t) \delta l_2(t-\tau) \rangle_t e^{-2\pi i \tau f} d\tau, \quad (1)$$

where the subscripts denote interferometers 1 and 2 (see Fig. 1), $f$ is frequency, and $\langle\rangle_t$ represents a time average over extended signal streams. Equation (1) can be equivalently expressed in units of strain as $\mathrm{CSD}_{\delta h} = \mathrm{CSD}/L^2$, which has the dimensionality of inverse frequency, or time. For frequencies in the 100 kHz to 20 MHz band, the interferometer signals are calibrated to absolute length to better than 1% statistical uncertainty with 5–7% systematic uncertainty, limited by the linearity of the photoreceivers. The spectral densities are estimated via Welch's periodogram method [23] using a Hann window, 50% overlapped segments, and a discrete Fourier transform size of $N_{\mathrm{DFT}} = 2^{16}$. The resulting 763 Hz wide frequency bins are subsequently rebinned to 9.92-kHz resolution via frequency-space averaging, accounting for the bin-to-bin covariance due to spectral leakage. Each 9.92-kHz frequency bin thus constitutes an independent measurement. Details about the data pipeline and signal calibration are described in §5 and §7 of Ref. [1], respectively.

Figure 2 shows the spectral averages of 1098 hours of dual interferometer time series data, collected in five observing runs from April 2017 to August 2019. All runs are found to be statistically consistent with one another, and their chronology is detailed in the Supplemental Material [22]. The power spectral densities, or auto spectra, of the individual interferometer signals (teal and green curves, top panel) are dominated by laser amplitude and phase noise and mechanical (seismic) noise below 1.1 MHz and by photon shot noise at higher frequencies. The lines spaced every 3.85 MHz are transmission resonances of the power-recycling cavity (free spectral ranges), at which frequencies input laser noise sidebands transmit to the antisymmetric port unattenuated. The weaker set of features spaced every 225 kHz in the auto spectra are thermally excited bulk modes of the fused silica substrates of the end mirrors, bend mirror, and beamsplitter.

In the CSD of the two interferometer signals (red curves or data points, all panels), these uncorrelated sources of noise are averaged down over $3.9 \times 10^{10}$ independent spectral measurements per 9.92-kHz bin to attain a sensitivity more than five orders of magnitude below the quantum sensing limit of either instrument individually.

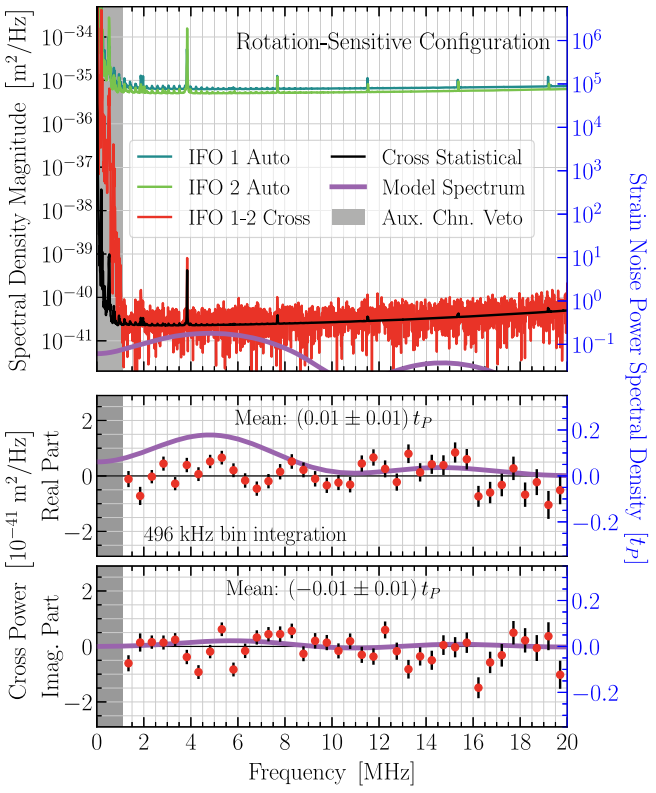


FIG. 2. Measured power and cross-spectral densities of the interferometer signals, shown in displacement units (left axis) and in strain units normalized to Planck time (right axis). The spectra are averaged across 1098 hours of dual interferometer time series data, or $3.9 \times 10^{10}$ independent spectral measurements per 9.92-kHz bin. Top panel: spectra magnitudes at 9.92-kHz resolution. The teal and green curves show the power spectral density of each interferometer (IFO). The red curve shows the cross-spectral density (CSD), whose statistical sensitivity is indicated by the black trace. Bottom panels: real and imaginary CSD components, rebinned to 496-kHz resolution. Error bars reflect the combined $1\sigma$ statistical uncertainty and 10% systematic calibration uncertainty [1]. For reference, all panels are overlaid with a semiclassical model spectrum of quantum geometrical fluctuations (purple curves) reproduced from Ref. [7], but adjusted for the actual dimensions of the as-built instrument. Bins showing excess coherence with environmental channels are vetoed (gray shading).

Overall, the noise level is flat, but rises slightly at higher frequencies due to phase noise between the two independent sample clocks, which leads to a growing decoherence between the digitized interferometer signals with higher frequency [1]. The excess coherence in noise below 1.1 MHz is due to laser technical noise correlations, as measured with auxiliary sensors; therefore, this band is excluded from analysis. A small number of frequency bins near cavity resonances are also excluded at higher frequencies on the basis of exhibiting an excess coherence with laser noise monitors, resulting in a total of $N = 1728$ science-quality frequency bins up to 20 MHz at 9.92-kHz resolution. Our full suite of data quality tests are detailed in §8 of Ref. [1]. Several enhancements of these tests are summarized in the Supplemental Material [22].

The measured complex CSD is consistent with no correlated displacement noise over the 1.1 MHz–20 MHz band. This is seen in the final result (Fig. 2, bottom panels), where we present the data rebinned to 496 kHz resolution for easier visual interpretation of signal to noise, utilizing the statistical independence of the 9.92-kHz bins (each observing run is also found to be consistent with this null result). Band averaged from 1.1 MHz to 20 MHz, the real and imaginary components of the final CSD are $(0.01 \pm 0.01)t_P$ and $(-0.01 \pm 0.01)t_P$, respectively, in units of strain noise power spectral density. The error bars represent the combined $1\sigma$ statistical uncertainty and 10% systematic calibration uncertainty [1]. The real and imaginary CSD components are considered separately because both conventional rf backgrounds and novel fields (e.g., axionlike couplings [5]) will generally couple to the interferometers in phase. In this case, correlated displacement noise will manifest entirely in the real quadrature, halving the number of sensitive degrees of freedom and thus the measurement variance. Correlations arising from holographic quantum geometry [7], on the other hand, depend on the antenna response to the nonlocally fluctuating background and can manifest in both quadratures. Within the 1.1 MHz–20 MHz band, we place an average limit of $3.72 \times 10^{-41}$ m$^2$/Hz $\approx 0.46 t_P L^2$ on the magnitude of stationary sources with bandwidth $\Delta f > 9.92$ kHz. For a white broadband stationary noise spanning the entire band, this limit improves to $1.03 \times 10^{-42}$ m$^2$/Hz.

*Model testing.*—We use this measurement to test a semiclassical model of instrument response to conjectured coherent, spacelike rotational fluctuations arising from quantum geometry. We adopt the prediction as in Ref. [7], but recalculated for the as-built instrument to account for slight differences in optical distances. The resulting model spectrum is shown in Fig. 2 (purple curves, all panels). Its magnitude scales with a normalization parameter, nominally $\eta \approx t_P$, which conveys a spectral density of information: along any timelike world line, $\eta$ is, heuristically, the unit time for each independent quantum "bit" to be defined. Its inverse regulates the scaling of directional uncertainties in the local inertial frames of causal diamonds and the entropies associated with the boundaries [7]. We constrain such rotational uncertainties using cross-interferometer CSD data from 1.1 MHz to 20 MHz to place an upper limit on $\eta$.

To obtain this limit, we perform a likelihood-ratio test. For two shot noise–dominated signals, the noise in each quadrature of the CSD is independent and Gaussian distributed. Using this fact, the likelihood ratio of a given model normalization to the $\eta = 0$ (classical spacetime) case assumes a simple form,

$$\Lambda(\eta) \equiv \exp\left(-\frac{1}{2}[\chi^2(\eta) - \chi^2(0)]\right), \tag{2}$$

where

$$\chi^2(\eta) = \sum_{k=1}^{N}\left[\frac{[\mathrm{Re}\, D(f_k) - \mathrm{Re}\, M(f_k,\eta)]^2}{\mathrm{Var}[\mathrm{Re}\, D(f_k)]} + \frac{[\mathrm{Im}\, D(f_k) - \mathrm{Im}\, M(f_k,\eta)]^2}{\mathrm{Var}[\mathrm{Im}\, D(f_k)]}\right] \tag{3}$$

is the $\chi^2$ statistic of the complex spectral model. In Eq. (3), $D$ refers to the CSD data (Fig. 2, red data points) and $M$ to the model prediction (the nominal case, $\eta = t_P$, is shown in purple curves). By Wilks' theorem, the difference in $\chi^2$ values, $\chi^2(\eta) - \chi^2(0)$, is asymptotically $\chi^2$ distributed with a single degree of freedom. This allows a direct estimation of the statistical significance. At 95% confidence we constrain the normalization to $\eta < 0.25 t_P$ for rotations around one axis, corresponding to a model with information content exceeding the conjectured bound from holographic entropy.

*Conclusions.*—Our results demonstrate a new frontier in precision measurement. For the first time, high-frequency differential lengths ($\delta l$) in a pair of large interferometers are used to measure a rotational degree of freedom. In coupling rotations of the system to the differential arm length, the bent-arm interferometers (see Fig. 1) sense an observable that is physically distinct from both the previous Holometer instrument and gravitational wave detectors. For stationary sources with bandwidth $\Delta f > 10$ kHz, the sensitivity to rotation-induced strain surpasses $\mathrm{CSD}_{\delta h} < t_P/2$ across a broad band from 1.1 MHz to 20 MHz. By averaging down the dominant, incoherent sources of interferometer noise over $3.9 \times 10^{10}$ independent spectral measurements per 9.92-kHz bin, we attain a sensitivity to coherent displacement noise power five orders of magnitude below the quantum sensing limit of either interferometer individually. Most importantly, we demonstrate with this technique that high-frequency environmental mitigation is possible (see the Supplemental Material [22] and Ref. [1]), enabling experimental sensitivities well beyond the threshold needed to test phenomenological models of holographic quantum spacetimes [7] and couplings of axionlike dark matter fields [5]. The use of quantum optical techniques may enhance the sensitivity even further [24,25].

The data presented here are consistent with a classical spacetime. They constrain a specific kind of departure from classicality—spacelike coherent, rotational quantum fluctuations about a single axis [7]—that would not have been detected before. Models of quantum gravity based on locally quantized fields on classical backgrounds predict no detectable effect in this type of measurement. Even so, searches for nonstandard, nonlocal quantum-geometrical effects are well motivated. Frameworks built on classical locality have well-known theoretical difficulties, such as accounting for information flow in the context of black hole horizons [11,12,26,27] and the small value of the cosmological constant [9,28–30]. Radical proposed modifications that address these issues, such as scale-invariant coherent geometrical states on causal diamonds, holographic nonlocal correlations, or geometrical "squeezing" [13–15], often produce large fluctuations on the displacement scale probed here, $\mathrm{CSD}_{\delta h} \sim t_P$. Our results significantly constrain such nonstandard options with a precision far exceeding limits currently achieved by other techniques, such as optical clocks [31,32].

Even though our measurement exceeds Planck sensitivity, it does not exclude all theories with large, nonlocally coherent holographic correlations. All light paths in our interferometers lie in a single plane. This configuration does not test models with Planck-scale uncertainty that entangles all three spatial directions; for example, it cannot coherently compare rotational states in orthogonal directions that may be associated with incompatible observables. Such models, if experimentally confirmed at Planck spectral density, may explain apparent anomalous symmetries in the cosmic microwave background [33–35] (for example, angular correlations of CMB temperature anisotropy, the only measurement to date of quantum correlations on the scale of a causal horizon, appear to exactly vanish at an angular separation of 90 degrees). A future experiment [20] is planned in a general 3D geometrical configuration to probe this class of theories. A quantitative assessment of new experimental designs thus motivated, as well as a thorough theoretical interpretation of our current result, will follow in future work.

This work was supported by Fermi National Accelerator Laboratory (Fermilab), a U.S. Department of Energy, Office of Science, HEP User Facility, managed by Fermi Research Alliance, LLC, acting under Contract No. DE-AC02-07CH11359. We are grateful for support from the John Templeton Foundation, the University of Chicago-Fermilab Strategic Collaborative Initiatives program, and the Fermilab Laboratory Directed Research and Development program. J. R. was partially supported by the Visiting Scholars Award Program of the Universities Research Association (Grant No. 18-S-20). O. K. was partially supported by the Basic Science Research Program (Grant No. NRF-2016R1D1A1B03934333) of the National Research Foundation of Korea funded by the Ministry of Education. The Holometer team gratefully acknowledges the extensive support and contributions of Gregory L. Brown, Andrea Bryant, Erin Glynn, Raymond H. Lewis, Arlo Marquez-Grap, Jeronimo Martinez, Matthew Quinn, James E. Ranson, Eleanor Rath, George Ressinger, and Michael Shemanske in the construction and operation of the apparatus. We also thank Rana Adhikari and Hartmut Grote for insightful comments during the data analysis and interpretation.

*kwon@uchicago.edu


[1] A. Chou, H. Glass, H. R. Gustafson, C. Hogan, B. L. Kamai, O. Kwon, R. Lanza, L. McCuller, S. S. Meyer, J. Richardson, C. Stoughton, R. Tomlin, and R. Weiss (Holometer Collaboration), The Holometer: An instrument to probe Planckian quantum geometry, Classical Quantum Gravity **34**, 065005 (2017).

[2] A. S. Chou, R. Gustafson, C. Hogan, B. Kamai, O. Kwon, R. Lanza, L. McCuller, S. S. Meyer, J. Richardson, C. Stoughton, R. Tomlin, S. Waldman, and R. Weiss (Holometer Collaboration), First Measurements of High Frequency Cross-Spectra From a Pair of Large Michelson Interferometers, Phys. Rev. Lett. **117**, 111102 (2016).

[3] A. Chou, H. Glass, H. R. Gustafson, C. J. Hogan, B. L. Kamai, O. Kwon, R. Lanza, L. McCuller, S. S. Meyer, J. W. Richardson, C. Stoughton, R. Tomlin, and R. Weiss (Holometer Collaboration), Interferometric constraints on quantum geometrical shear noise correlations, Classical Quantum Gravity **34**, 165005 (2017).

[4] A. S. Chou, R. Gustafson, C. Hogan, B. Kamai, O. Kwon, R. Lanza, S. L. Larson, L. McCuller, S. S. Meyer, J. Richardson, C. Stoughton, R. Tomlin, and R. Weiss (Holometer Collaboration), MHz gravitational wave constraints with decameter Michelson interferometers, Phys. Rev. D **95**, 063002 (2017).

[5] H. Grote and Y. V. Stadnik, Novel signatures of dark matter in laser-interferometric gravitational-wave detectors, Phys. Rev. Research **1**, 033187 (2019).

[6] C. Hogan, Exotic rotational correlations in quantum geometry, Phys. Rev. D **95**, 104050 (2017).

[7] C. Hogan, O. Kwon, and J. Richardson, Statistical model of exotic rotational correlations in emergent space-time, Classical Quantum Gravity **34**, 135006 (2017).

[8] M. Zych, F. Costa, I. Pikovski, and Č. Brukner, Bell's theorem for temporal order, Nat. Commun. **10**, 3772 (2019).

[9] A. G. Cohen, D. B. Kaplan, and A. E. Nelson, Effective Field Theory, Black Holes, and the Cosmological Constant, Phys. Rev. Lett. **82**, 4971 (1999); A. G. Cohen and D. B. Kaplan, Gravitational contributions to the electron $g$-factor, arXiv:2103.04509.

[10] T. Banks and W. Fischler, The holographic spacetime model of cosmology, Int. J. Mod. Phys. D **27**, 1846005 (2018); T. Banks, Holographic space-time and quantum information, Front. Phys. **8**, 111 (2020).

[11] G. 't Hooft, Virtual black holes and space–time structure, Found. Phys. **48**, 1134 (2018).

[12] S. B. Giddings, Black holes in the quantum universe, Phil. Trans. R. Soc. A **377**, 20190029 (2019).

[13] E. P. Verlinde and K. M. Zurek, Observational signatures of quantum gravity in interferometers, arXiv:1902.08207.

[14] E. P. Verlinde and K. M. Zurek, Spacetime fluctuations in AdS/CFT, J. High Energy Phys. 04 (2020) 209.

[15] M. Parikh, F. Wilczek, and G. Zahariade, The noise of gravitons, Int. J. Mod. Phys. D **29**, 2042001 (2020); Quantum mechanics of gravitational waves, arXiv:2010.08205.

[16] D. Carney, P. C. E. Stamp, and J. M. Taylor, Tabletop experiments for quantum gravity: A user's manual, Classical Quantum Gravity **36**, 034001 (2019).

[17] R. Howl, V. Vedral, D. Naik, M. Christodoulou, C. Rovelli, and A. Iyer, Non-gaussianity as a signature of a quantum theory of gravity, PRX Quantum **2**, 010325 (2021).

[18] T. Jacobson, Thermodynamics of Spacetime: The Einstein Equation of State, Phys. Rev. Lett. **75**, 1260 (1995).

[19] T. Jacobson, Entanglement Equilibrium and the Einstein Equation, Phys. Rev. Lett. **116**, 201101 (2016).

[20] S. Vermeulen, L. Aiello, A. Ejlli, W. Griffiths, A. James, K. Dooley, and H. Grote, An experiment for observing quantum gravity phenomena using twin table-top 3D interferometers, Classical Quantum Gravity **38**, 085008 (2021).

[21] E. D. Black, An introduction to Pound–Drever–Hall laser frequency stabilization, Am. J. Phys. **69**, 79 (2001).

[22] See Supplemental Material at http://link.aps.org/supplemental/10.1103/PhysRevLett.126.241301 for updated limits on environmental noise couplings, detailed descriptions of those measurements, and a chronology of our science data runs.

[23] P. Welch, The use of fast fourier transform for the estimation of power spectra: A method based on time averaging over short, modified periodograms, IEEE Trans. Audio Electroacoust. **15**, 70 (1967).

[24] I. Ruo Berchera, I. P. Degiovanni, S. Olivares, and M. Genovese, Quantum Light in Coupled Interferometers for Quantum Gravity Tests, Phys. Rev. Lett. **110**, 213601 (2013).

[25] S. T. Pradyumna, E. Losero, I. Ruo-Berchera, P. Traina, M. Zucco, C. S. Jacobsen, U. L. Andersen, I. P. Degiovanni, M. Genovese, and T. Gehring, Twin beam quantum-enhanced correlated interferometry for testing fundamental physics, Commun. Phys. **3**, 104 (2020).

[26] G. 't Hooft, Black hole unitarity and antipodal entanglement, Found. Phys. **46**, 1185 (2016).

[27] T. Banks and W. Fischler, Cosmological Implications of the Bekenstein Bound, in *Jacob Bekenstein*, edited by L. Brink, V. Mukhanov, E. Rabinovici, and K. K Phua (World Scientific, Singapore, 2019), pp. 121–138.

[28] S. Weinberg, The cosmological constant problem, Rev. Mod. Phys. **61**, 1 (1989); *Cosmology* (Oxford University Press, New York, 2008).

[29] T. Banks and W. Fischler, Why the cosmological constant is a boundary condition, arXiv:1811.00130.

[30] C. Hogan, Cosmological constant in coherent quantum gravity, Int. J. Mod. Phys. D **29**, 2042004 (2020).

[31] S. L. Campbell, R. B. Hutson, G. E. Marti, A. Goban, N. Darkwah Oppong, R. L. McNally, L. Sonderhouse, J. M. Robinson, W. Zhang, B. J. Bloom, and J. Ye, A Fermi-degenerate three-dimensional optical lattice clock, Science **358**, 90 (2017).

[32] G. Wendel, L. Martínez, and M. Bojowald, Physical Implications of a Fundamental Period of Time, Phys. Rev. Lett. **124**, 241301 (2020).

[33] C. Hogan, Nonlocal entanglement and directional correlations of primordial perturbations on the inflationary horizon, Phys. Rev. D **99**, 063531 (2019).

[34] C. Hogan, Pattern of perturbations from a coherent quantum inflationary horizon, Classical Quantum Gravity **37**, 095005 (2020).

[35] R. Hagimoto, C. Hogan, C. Lewin, and S. S. Meyer, Symmetries of CMB temperature correlation at large angular separations, Astrophys. J. **888**, L29 (2020).